Solidification Cracking Susceptibility of Welding Fillers Derived from Scrap Aluminum — Part 1: Powder Core Wire Experiments

Filler materials derived from aluminum scrap have the potential for greater weldability and higher hardness compared to existing precipitation-hardened alloys

BY J. HAMILTON, J. E. CARSLEY AND J. KLEMM-TOOLE

Abstract

Sustainable material production is becoming increasingly desirable for providing decreased energy consumption and emissions. The twitch aluminum scrap stream is high in elements such as Si, Fe, Cu, and Mg, which can pose challenges to reuse in existing alloys. Alternatively, it may be possible to use twitch to produce a novel wire feedstock for additive manufacturing and welding if compositions can be identified or engineered to resist solidification cracking. This study investigates the susceptibility of twitch-derived alloys to solidification cracking compared with commercially available alloys such as 6061, 4043, and 5356. Although predictions from solidification cracking criteria indicate that the twitch alloys should be more crack resistant than the commercial alloys, the results of Sigmajig weldability tests revealed that the twitch alloys were more crack resistant than 6061 but not 4043 or 5356. The lower-than-expected weldability of the twitch alloys was attributed to oxides present in the welds, resulting from the powder core tubular wiremaking process used to produce these novel feedstocks. Despite lower weldability, welds from the twitch fillers exhibited considerably higher hardness than those of the other materials, indicating great potential to develop high-strength, weldable compositions from the aluminum scrap stream.

https://doi.org/10.29391/2026.105.023

Keywords

- Welding Fillers
- Weldability
- Aluminum Alloys
- Gas Tungsten Arc Welding
- Mechanical Behavior

Introduction

Integrating more recycling streams into aluminum (Al) production would improve sustainability and reduce emissions. Currently, Al production from bauxite ore is among the most energy and carbon intensive metallurgical processes (Refs. 1–3). Aluminum production accounts for ~3% of all greenhouse gas emissions and 15% of emissions in the industrial sector (Refs. 1, 4). Additionally, production from bauxite consumes ~126 GJ of energy per ton, with approximately 80,500 tons of Al produced globally in 2024 (Refs. 5, 6). Therefore, finding a way to increase the use of recycled Al will decrease emissions and improve energy efficiency. The twitch scrap stream contains wrought and recycled Al from the automotive industry (Refs. 1, 7, 8). The composition of the twitch scrap stream varies across the country but is generally within the ranges listed in Table 1 (Refs. 7–9). The twitch scrap stream is considered end of life because excessive alloying elements such as Si, Fe, Cu, and Mg inhibit its recyclability into wrought products. It may be possible to convert the remaining (lower-value) twitch scrap into a value stream by producing wire feedstock for additive manufacturing and welding. Additionally, producing wire feedstock from the twitch scrap stream is made more challenging due to limited compositional control.

Table 1 — Compositional Ranges of Different Elements in the Twitch Scrap (Ref. 9)

Element	Si	Fe	Cu	Mn	Mg	Cr	Ni	Zn	Ti	Res.	Al
Range (wt–%)	1–9	0.3–0.7	0.3–4	0.09–0.4	0.3–12	0–0.1	0–0.3	0.1–3	0–0.1	<0.01	Bal.
Average(wt–%)	5.28	0.53	1.63	0.24	1.79	0.04	0.07	1.06	0.04	<0.01	Bal.

Al and its alloys are particularly susceptible to solidification cracking due to large solidification shrinkage and thermal contraction (Refs. 10–12). 6xxx-series Al alloys are highly crack susceptible, for example, because of the large temperature range over which little solid forms during terminal solidification (Refs. 13–15). Alloying can help reduce susceptibility to cracking by modifying eutectic reactions during terminal solidification (Refs. 10, 11, 13, 16). Si and Mg promote fluidity in Al alloy systems, and Cu and Si promote eutectic reactions, all of which help reduce solidification cracking susceptibility (Refs. 11, 17–20). Cracking can also be mitigated by the formation of fine equiaxed grains during solidification (Refs. 16, 21–24). Alloys like 4043 and 5356 are suitable weld fillers because of their elevated Si and Mg contents, promoting fluidity and eutectic reactions. It may be possible to create a wire feedstock derived from the twitch scrap stream because, as shown in Table 1, it contains elevated amounts of Si, Cu, and Mg.

This paper seeks to explore the solidification cracking behavior in twitch-derived alloys with compositions selected from the elemental ranges given in Table 1 and to compare it with that of 6061, 4043, and 5356. Models are used to predict differences in the tendency for solidification cracking between the twitch based alloys and commercial fillers, and the fillers' susceptibility to solidification cracking is evaluated using the Sigmajig weldability test. The microstructure and hardness after solidification of the various filler materials are compared. The results of this work are expected to shed light on the potential of using scrap Al as filler materials for welding and additive manufacturing.

Methods

Predicting Solidification Cracking Behavior

Solidification cracking is a primary concern when using Al-based fillers for welding and fusion based additive manufacturing (Refs. 10, 15). Therefore, it is important to understand the susceptibility of candidate filler materials to solidification cracking, and various models can be used to predict cracking behavior. Kou developed the cracking susceptibility index (CSI), which predicts that solidification cracking susceptibility increases as the steepness of the Scheil curve increases at terminal solidification (Refs. 10, 11, 25). The CSI is considered to be the maximum slope in a temperature vs (volume fraction of solid)$^{1/2}$ within the range of 0.85–0.99 (volume fraction of solid)$^{1/2}$ as shown in Equation 1, where T is temperature (K) and f_s is volume fraction of solid.

$$CSI = Max \left| \frac{dT}{df_s^{1/2}} \right|, 0.85 > f_s^{1/2} > 0.99 \quad (1)$$

Kou argues that solidification cracking occurs when lateral strains across the solidifying material pull dendrites apart faster than dendrites can coalesce and the liquid can backfill the gaps between them (Ref. 11).

Another model developed by Giorjao et al. analyzes liquid backfilling behavior using Scheil curves to model solidification morphology and create a "funnel" between two dendrites (Ref. 26). The funnel can be used to calculate the liquid pressure drop as it flows between the solidifying dendrites. A higher pressure drop increases flow resistance and susceptibility to solidification cracking (Refs. 26, 27). This model, referred to as the flow resistance index (FRI), is given by Equation 2 below, where μ is the dynamic viscosity.

$$FRI = \sum_{f_s=0.85}^{0.98} \frac{\mu}{(1-\sqrt{f_s})^4} \quad (2)$$

Thermo-Calc 2024a with the TCAL9 database was used to generate Scheil curves and calculate the dynamic viscosity of the liquid during solidification for the CSI and FRI models. The modeling was then used to qualitatively compare the susceptibility of the different alloys to solidification cracking.

Filler Materials

The compositions of the twitch-based fillers were replicated using a powder core tubular wire mill. A 2024 Al strip sheath was used, and various powders were added to achieve the compositions shown in Table 2. The compositions were identified using optical emission spectroscopy (OES) on the deposited Sigmajig samples. Each twitch wire was drawn to a ⅛-in. diameter. Details of the powder core tubular wire making are provided elsewhere (Ref. 9). Nominal twitch is intended to represent an average composition of the twitch scrap stream. In contrast, HiSi twitch is intended to explore whether elevated Si can reduce cracking by increasing fluidity and/or promoting more eutectic reactions. These alloys were chosen to represent the complex composition of the scrap stream. Both compositions were designed based on the ranges in Table 1 and on their predicted susceptibilities to solidification cracking from the CSI and FRI models.

The 4043 and 5356 commercial filler materials used were AWS A5.10/ASME SFA-5.10 R4043 and R5356 Al TIG rods. Each rod was 1/16 in. × 36 in. The nominal compositions of 4043, 5356, and 6061 are listed in Table 2.

Table 2 — Nominal and HiSi Twitch Compositions for Samples Manually Deposited from Powder-Core Tubular Wire, Alongside Nominal Compositional Details (wt-%) of 4043, 5356, and 6061, as Listed in ASTM and AWS Standards, and Provided by Lincoln Electric (Refs. 28-30)

Alloy	Si	Fe	Cu	Mn	Mg	Cr	Ni	Zn	Ti
Nominal Twitch	0.52	0.27	3.58	0.45	1.16	0.01	0.01	0.09	0.02
HiSi Twitch	2.94	0.51	2.87	0.33	0.92	0.01	0.01	0.07	0.02
4043	4.5–6.0	<0.8	<0.3	<0.05	<0.05	–	–	<0.1	<0.2
5356	<0.25	<0.4	<0.1	0.05–0.2	4.5–5.5	0.05–0.2	–	<0.1	0.06–0.2
6061	0.4–0.8	0.7	0.15–0.4	0.15	0.6–1.2	0.04–0.35	–	0.25	0.15

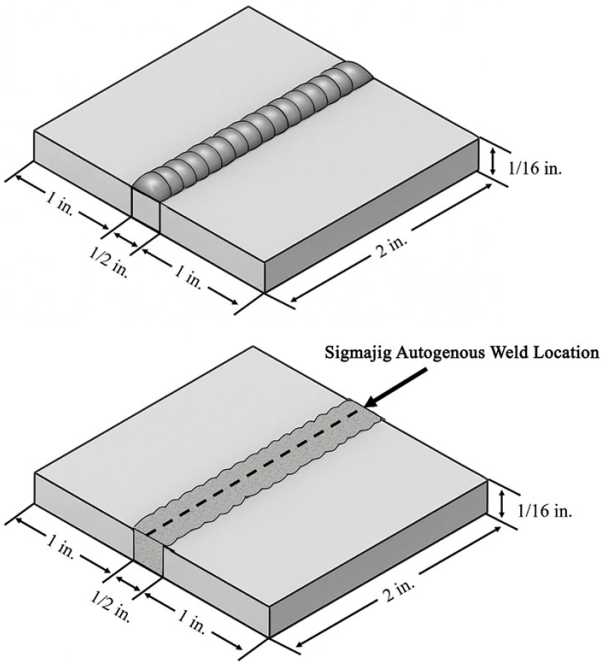


Fig. 1 — Representation of how the Sigmajig samples were produced. A ½-in. root gap was filled with a specified filler material, the welds were manually machined flush with the base plate, and the autogenous weld during the Sigmajig test was performed on the filler metal region.

Sigmajig Weldability Testing

Sigmajig test specimens were produced by using the filler materials to weld a ½-in. gap between two 1⁄16-in. thick 6061 plates using a Miller Dynasty GTAW machine, as shown in Fig. 1. During manual deposition, the current fluctuated between 25 and 150 A, with an average deposition rate of 2 mm/s. The filler was deposited on both sides of the plates to prevent lack-of-fusion defects. The weld buildup was machined down so that the deposited material was flush with the 6061 plate, and the samples were consistently 1⁄16-in. thick. To evaluate the weldability of 6061, 1⁄16-in. 6061 plates were used. All specimens were cut to 2-in. × 2-in. × 1⁄16-in. for testing.

The samples were mounted in the Sigmajig test apparatus (Ref. 31), and various tensile loads were applied by tightening strain-gauged bolts with Belleville washers. A single autogenous GTAW pass was made on the region containing the weld made with filler material, where the welding parameters were 120 A, 10-12 V, and an arc length of 1.5 mm. Welding speed was controlled by a Rail Runner Gen III gantry track at 12 mm/s. All the materials were evaluated under identical welding parameters.

The cracking response was evaluated based on the length of the largest single centerline crack relative to the total weld length. This measurement was done using a DSX500 light optical microscope and the ImageJ software. On samples that experienced 100% cracking, the fracture surfaces were analyzed using a Tescan S8252G scanning electron microscope (SEM) at 15 keV to determine the fracture mode.

Hardness & Microscopy

The hardness of the alloy was measured using the Vickers microhardness test. Fifteen measurements were taken per sample on the melt track formed during Sigmajig testing. The grain size and morphology were determined through electron backscatter diffraction (EBSD) using a Tescan S8252G SEM with a beam energy of 15 keV. EBSD images were processed in MATLAB R2023a using MTEX to remove low-index data points where pores and cracks were present.

Results

Predictions of Solidification Cracking Behavior

Scheil curves for each material evaluated here are shown in Fig. 2. In general, the twitch alloys exhibited considerably more reactions toward the end of solidification than 6061, 4043, and 5356. Furthermore, due to the numerous terminal solidification reactions in the twitch alloys, the temperature

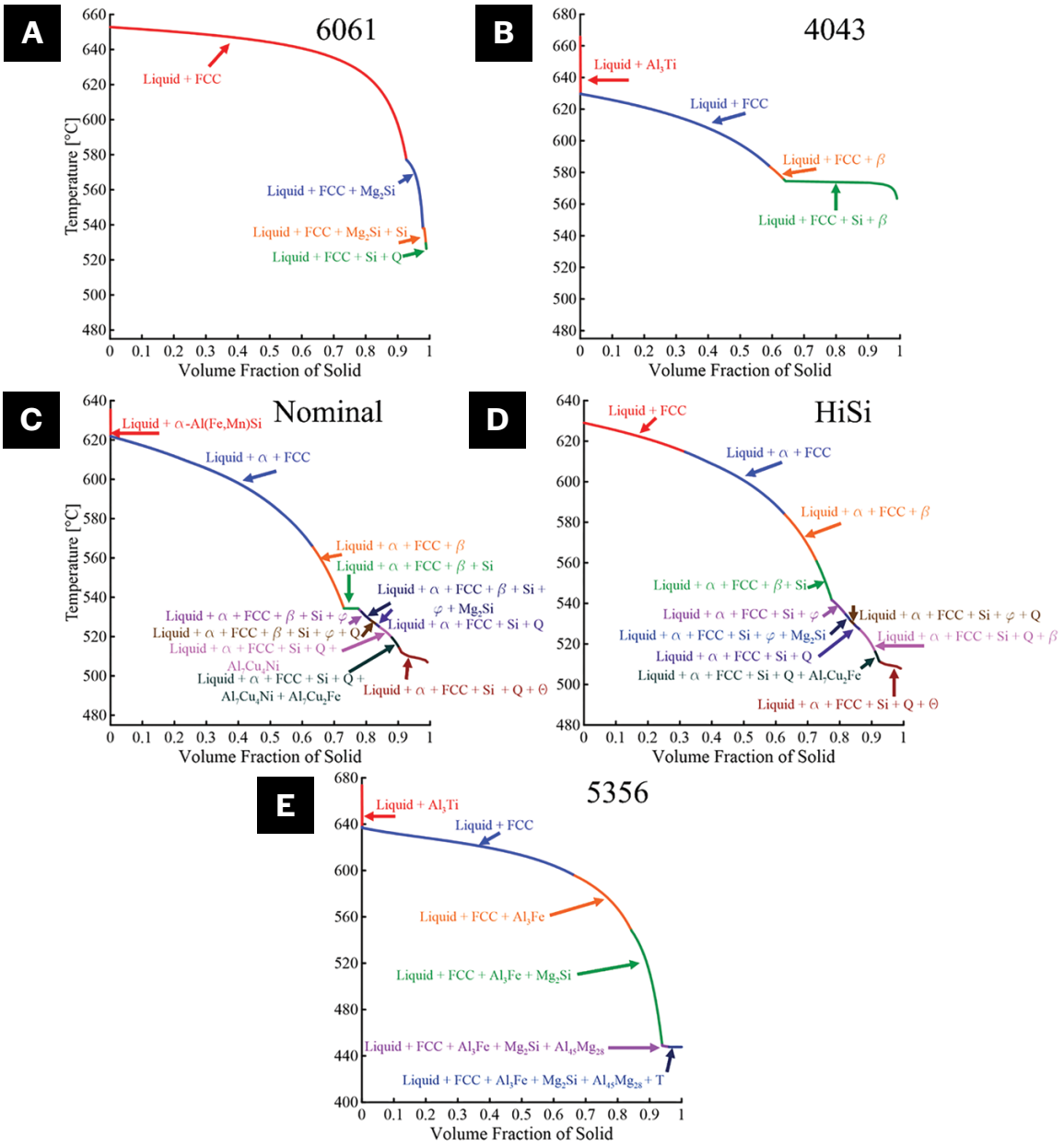


Fig. 2 — Temperature vs volume fraction of solid from Scheil simulations for: A — 6061; B — 4043; C — nominal twitch; D — HiSi twitch; E — 5356 alloys.

vs. volume fraction of solid curve is less steep than that of the commercial alloys, providing a preliminary indication of good weldability. The large amount of secondary phases formed at the end of solidification also indicate the potential for higher strength in the twitch alloys as well.

The results of the CSI and FRI models are shown in Fig. 3 below. Both models predict that 6061 should be the most susceptible to cracking, followed by 4043. The CSI model predicts that the next most susceptible alloy should be 5356, followed by Nominal twitch, with HiSi twitch the least susceptible. However, the FRI model predicts 5356 will be the least susceptible, followed by nominal twitch and HiSi twitch. The nominal twitch alloy is predicted to have a lower viscosity than the HiSi twitch alloy, which may explain some of the differences between the two alloys. The dynamic viscosities of the nominal and HiSi twitch alloys are also generally higher and increase at a higher rate than those of 4043 and 5356 toward terminal solidification. Both CSI and FRI use the slope of the Scheil curve at terminal solidification to determine susceptibility to solidification cracking. 5356 has a low dynamic viscosity that does not change substantially as temperature decreases, thereby counteracting the steeper slope of the Scheil curve in the FRI model. The viscosity of the terminal liquid in 4043 is relatively high, between 0.85 and 0.99 volume fraction of solid, and it has a steeper slope, which is likely why CSI and FRI both predict that it will have a higher susceptibility than that of twitch alloys and 5356.

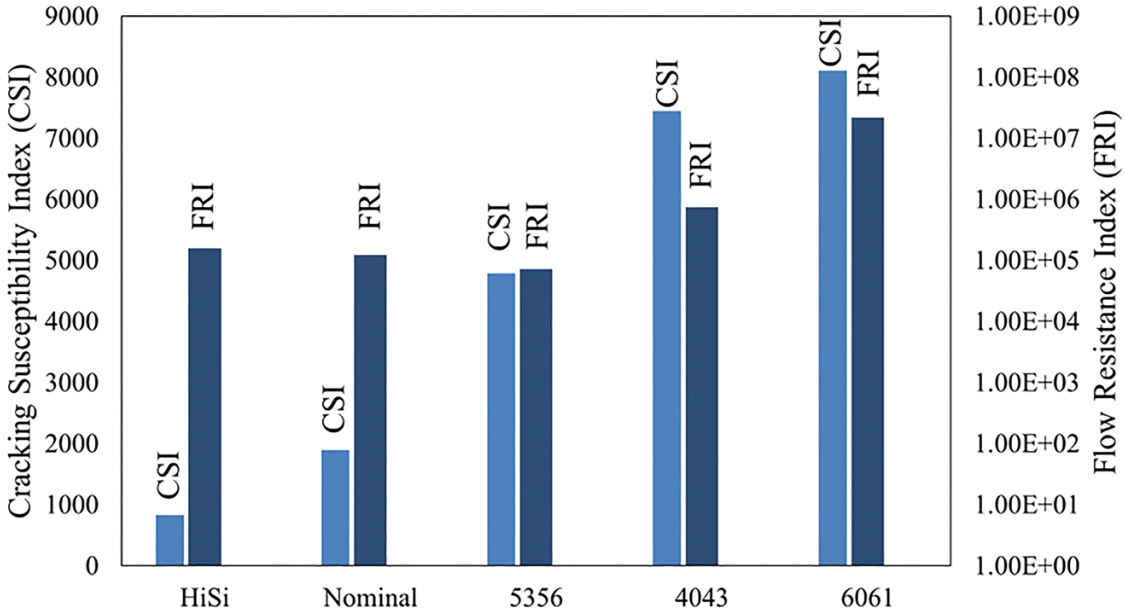


Fig. 3 — Predictions of the tendency for solidification cracking from the CSI and FRI models. Higher CSI and FRI correspond to a higher tendency for solidification cracking.

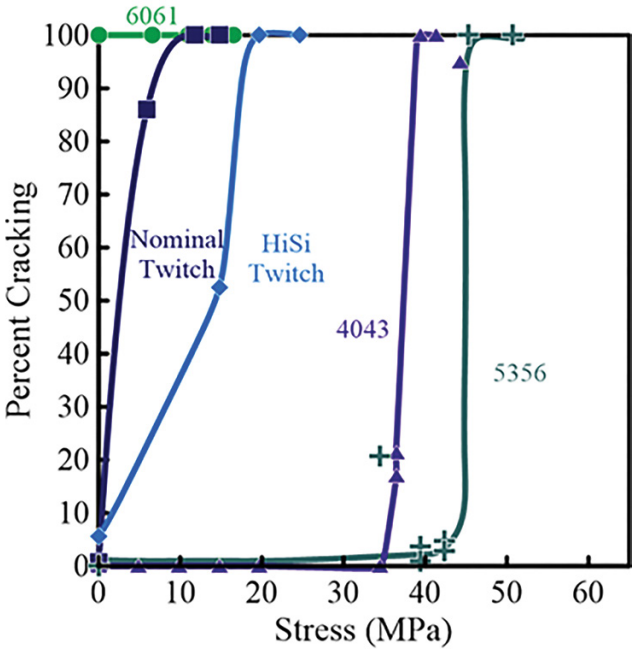


Fig. 4 — Solidification cracking results from Sigmajig testing. Percent cracking is determined as the longest crack in the fusion zone divided by the length of the sample.

Sigmajig

Samples of 6061, 4043, 5356, nominal twitch, and HiSi twitch were tested at a variety of stresses to determine the cracking behavior of each different alloy. Figure 4 shows the results of cracking vs applied stress. 6061 experienced 100% cracking under no applied stress. The thermal contraction during solidification was sufficient to cause complete cracking since 6061 is so susceptible to solidification cracking. The nominal and HiSi twitch alloys showed small cracks under no applied stress, but did not experience 100% cracking until approximately 12 MPa and 20 MPa, respectively. 4043 did not experience any cracking until an applied stress of approximately 36 MPa, and experienced 100% cracking at 40 MPa. 5356 had the greatest cracking resistance, with crack initiation occurring between 35 and 40 MPa, and 100% cracking at 45 MPa. Scatter in the data between 35 and 40 MPa makes it difficult to distinguish the onset of cracking for 5356.

Figure 5 shows macroscopic photos of samples from each alloy following Sigmajig testing. The melt tracks on the nominal and HiSi twitch samples in Figs. 5B and C show dark regions, which are oxides that floated to the surface during autogenous welding in the Sigmajig test. 6061, 4043, and 5356 show no significant oxidation. It should also be mentioned that many fine cracks originate from the oxide patches in the twitch alloys, which may be affecting the cracking response.

Microscopy was performed on the fracture surfaces of failed Sigmajig specimens. Figure 6 below shows an example SEM-SE fractography for the different alloys. Dendrites are clearly observable in all the samples, indicating that solidification cracking is the primary fracture mechanism in the Sigmajig samples. Both twitch alloys also show regions where dendrites are not visible on the fracture surface. These regions are near locations where oxides are present on the fracture surface, as shown in Fig. 7. Despite the different fracture appearance near oxides in the twitch samples, much of the fracture surface can be attributed to solidification cracking.

Grain Size in the Fusion Zone

Sigmajig samples were sectioned perpendicular to the torch travel direction to evaluate the grain size in the fusion zone using EBSD, and the results are shown in Fig. 8. The white spots are pores in all images. In general, the grains appear more columnar at the edge of the fusion zone (left) and more equiaxed at the center (right). However, the grains in the center of the fusion zone are likely still elongated but oriented perpendicular to and out of the sectioning plane. 6061 appears to have the most columnar grains at the edge of the fusion zone, followed by the twitch alloys, and then the other two commercial alloys. The average grain size of the samples is summarized in Table 3. HiSi twitch has the largest average grain diameter, followed by 6061, nominal twitch, 4043, and 5356. In addition to the inherent susceptibility to cracking indicated by the CSI and FRI models, the larger grain sizes in 6061, HiSi twitch, and nominal twitch may contribute to the greater degree of solidification cracking observed in Sigmajig testing.

Hardness in the Fusion Zone

Hardness was measured in the fusion zone of the Sigmajig samples, and Fig. 9 shows the hardness of the 5 different materials evaluated. Nominal twitch and HiSi twitch have higher hardness than all the other alloys evaluated. The high hardness of the twitch-based alloys indicates the potential to produce high-strength aluminum fillers from the aluminum scrap stream.

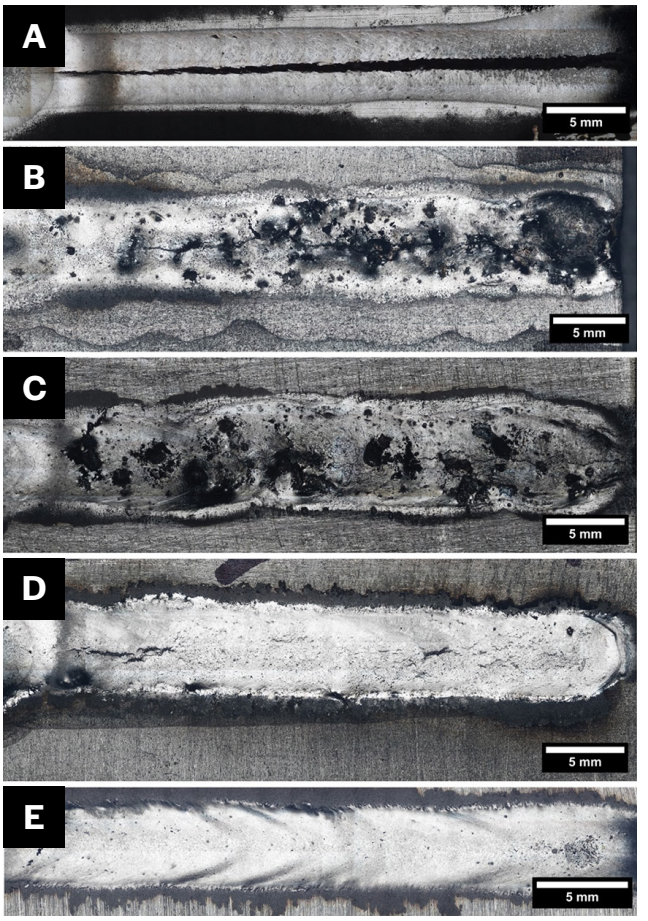


Fig. 5 — Macroscopic LOM images of the cracking in: A — 6061, 0 MPa; B — nominal twitch, 6 MPa; C — HiSi twitch, 15 MPa; D — 4043, 36 MPa; E — 5356, 39 MPa after Sigmajig testing.

Discussion

Comparison of Predicted and Experimental Solidification Cracking Susceptibility

The two models used to predict the susceptibility to solidification cracking capture two distinct aspects of cracking and were used together to compare the alloys. The CSI model predicts solidification behavior from the shape of the Scheil curve and suggests that the cracking susceptibility of the twitch alloys would be the lowest, followed by 5356, 4043, and 6061. However, the FRI model predicts cracking susceptibility based on the shape of the Scheil curve and the liquid's dynamic viscosity, and suggests that 5356 will have the lowest susceptibility, followed by the twitch alloys, then 4043 and 6061. Both models accurately predicted the ranking of 4043, 5356, and 6061 relative to each other, as shown by the Sigmajig results. It is worth noting that 4043 and 5356 exhibited high cracking resistance, which contributes to their popular use. The FRI model more accurately predicted that 5356 was the most resistant to solidification cracking. While many welders prefer to use 4043 over 5356 due to its ability to flow during welding (Ref. 32), 5356 has been documented to have better cracking resistance and finer grain sizes than 4043 when welding other Al systems (Refs. 33, 34). However, the fillers were welded with different parameters. The literature lacks direct comparisons of the weldability of 4043 and 5356 under identical conditions, so the Sigmajig results in this work represent a contribution to the field. Both CSI and FRI predicted that the twitch alloys should be less susceptible than 4043, but Sigmajig testing showed otherwise.

There are several possible reasons for the disparities between the modeling results and the experiments. Large columnar-grained and high-hardness materials tend to be more susceptible to solidification cracking (Refs. 11, 16). Materials with smaller, equiaxed grains in the fusion zone are more crack-resistant because solidification cracking is an intergranular cracking mechanism; therefore, equiaxed grains introduce a more tortuous crack-propagation pathway (Refs. 16, 21, 22). The results in Fig. 8 and Table 3 indicate that 6061 has the greatest concentration of columnar grains approaching the fracture surface and the second-largest grain size. HiSi twitch had the largest grain size, but still outperformed 6061, possibly because it had more equiaxed grains. The two twitch alloys also had the highest hardnesses and exhibited the greatest tendency for cracking, except for 6061. While hardness can be used as an indicator of susceptibility to solidification cracking, it provides only an incomplete assessment of the mechanical response of the twitch.

Even considering the potential influences of grain size/morphology and hardness, oxides in the melt tracks of the twitch alloys likely had the greatest additional influence on

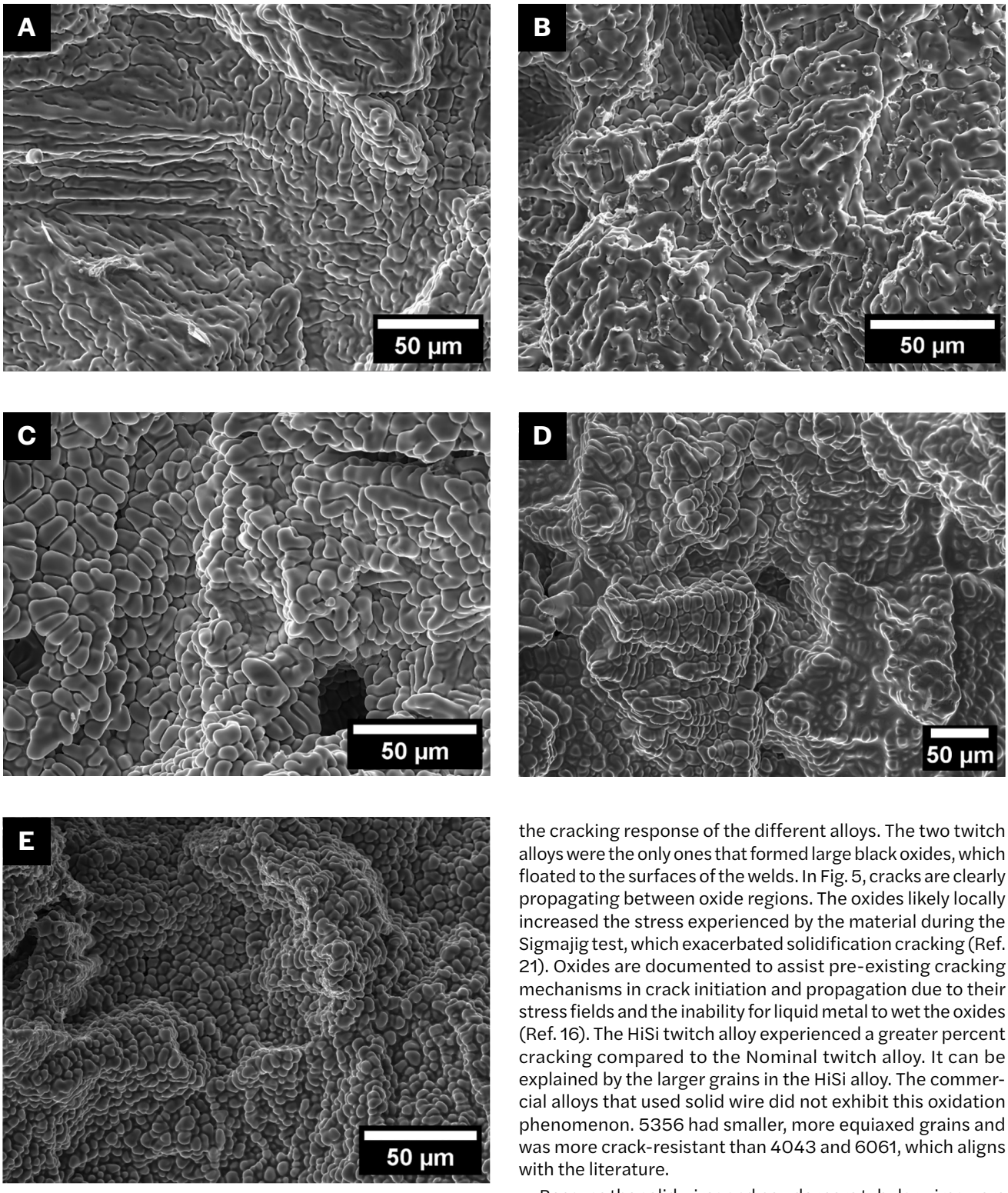


Fig. 6 — SEM SE fractography showing dendrites on the surface of the fracture surface for: A — 6061; B — nominal twitch; C — HiSi twitch; D — 4043; E — 5356, indicating solidification cracking was the primary failure mode.

the cracking response of the different alloys. The two twitch alloys were the only ones that formed large black oxides, which floated to the surfaces of the welds. In Fig. 5, cracks are clearly propagating between oxide regions. The oxides likely locally increased the stress experienced by the material during the Sigmajig test, which exacerbated solidification cracking (Ref. 21). Oxides are documented to assist pre-existing cracking mechanisms in crack initiation and propagation due to their stress fields and the inability for liquid metal to wet the oxides (Ref. 16). The HiSi twitch alloy experienced a greater percent cracking compared to the Nominal twitch alloy. It can be explained by the larger grains in the HiSi alloy. The commercial alloys that used solid wire did not exhibit this oxidation phenomenon. 5356 had smaller, more equiaxed grains and was more crack-resistant than 4043 and 6061, which aligns with the literature.

Because the solid wires and powder core tubular wires were welded under identical conditions, the source of the oxides (only present in the tubular wire) is likely from the powder core tubular wire making process. Powder core tubular wires were used to generate nominal and HiSi twitch samples as an efficient means of producing custom compositions. However, they have a lower density due to incomplete packing of the powder in the core. The powders are of different shapes and sizes, leaving empty pockets throughout the entire length of

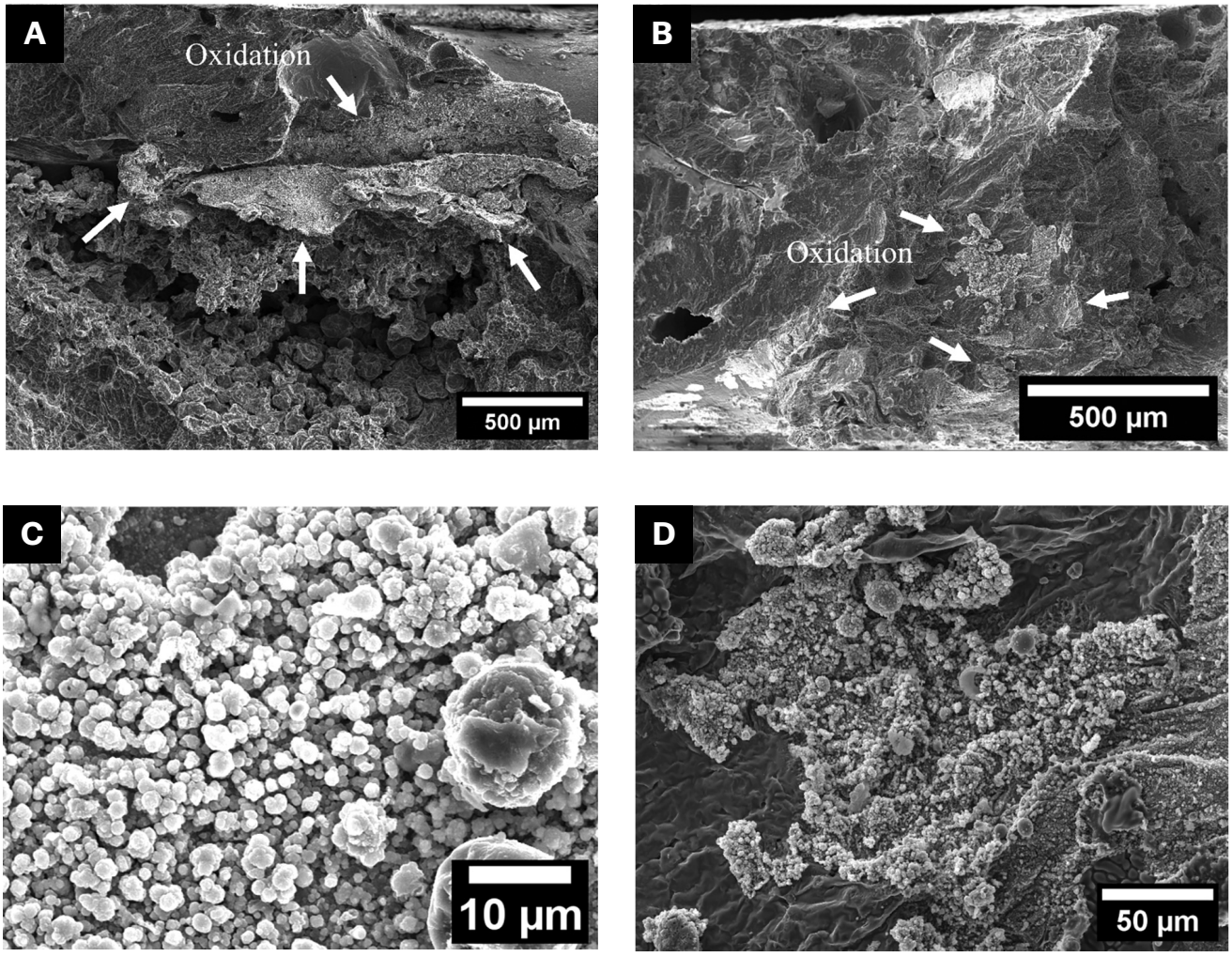


Fig. 7 — SEM SE images of oxidation present on the fracture surfaces of: A and C — Nominal twitch; B and D — HiSi twitch. C and D are higher-magnification images of the oxides indicated in A and B.

Table 3 — Average Grain Diameters in the Fusion Zone of Sigmajig Samples

Material	Average Grain Diameter (µm)
Nominal Twitch	128.3
HiSi Twitch	174.8
4043	109.4
5356	91.3
6061	146.6

the wire. Additionally, aluminum has a high affinity for oxygen, especially when in powder form, due to the increased surface area exposed to air (Refs. 35, 36). Lastly, during the wire drawing process, the wire is passed through a dry lubricant, which can get folded into the sheath or blended into the powder. Solid wires will generally have a greater density and fewer opportunities for oxygen to embed in the material. The solidification cracking response of the twitch alloys was likely strongly influenced by oxidation behavior, and future studies will use solid wire instead to prevent potential oxi-

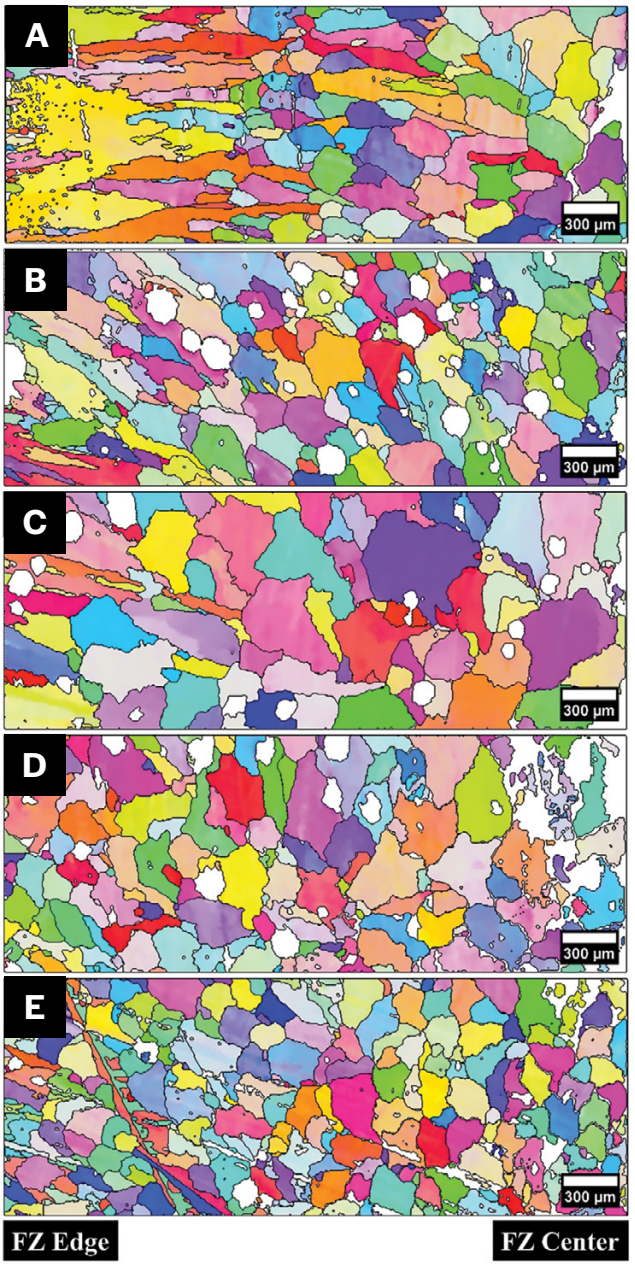


Fig. 8 — EBSD scans of the fusion zone from: A — 6061; B — nominal twitch; C — HiSi twitch; D — 4043; E — 5356 Sigmajig samples. The edge of the fusion zone (FZ) is on the left, and the center of the FZ where cracking occurred is on the right. White regions are pores or other features that the EBSD software could not index.

dation. This work revealed that powder core wire is not ideal for evaluating Al-based filler materials due to the propensity for oxidation. However, even with oxide-induced cracking in the twitch alloys, they exhibit higher hardness and reduced susceptibility to cracking compared to 6061, indicating significant potential for using scrap aluminum as a high-strength, sustainable welding filler.

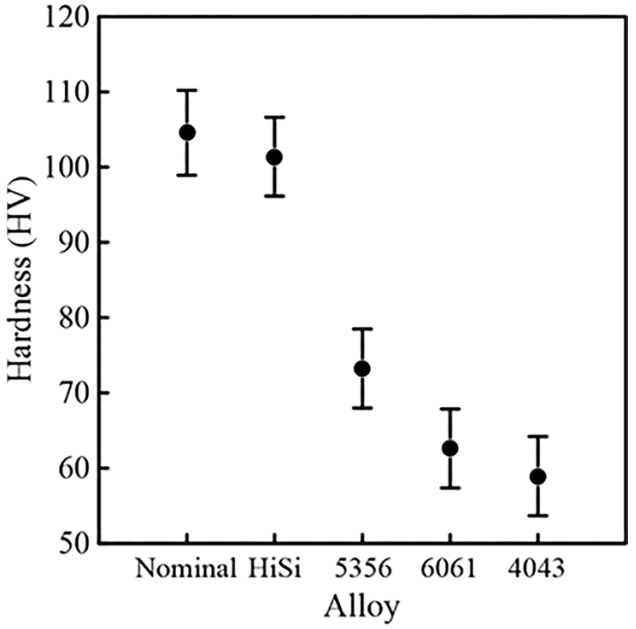


Fig. 9 — Average measured hardness of each material measured in the fusion zone of Sigmajig samples. Dots represent mean values, and error bars represent 95% confidence intervals.

Future Opportunities for Scrap-Based Aluminum Filler Materials

The results of this study suggest that it may be possible to make a solidification cracking-resistant weld filler derived from the twitch scrap stream with higher strength than existing fillers, though the method used to produce the filler wire significantly affects the performance of the alloy. The next stage of this research will utilize solid wire feedstocks to eliminate the influence of oxides in the melt pool. It will accompany this research as Part II of this publication series. Preliminary research suggests that solid twitch fillers have lower but comparable resistance to solidification cracking compared to 4043. CSI predictions in previous work (Ref. 9) indicate that the Cu content in the alloy has the most significant influence on the solidification cracking response, and future research will seek to determine the Cu content that optimally balances good weldability with a strong age hardening response. Overall, there appears to be great potential to utilize the twitch scrap stream to produce high-performance Al filler materials for structural applications.

Conclusions

This study examined the solidification cracking behavior of alloys derived from the twitch scrap stream, compared with the commercial materials 6061, 4043, and 5356. Cracking susceptibility was predicted using the CSI and FRI models and compared to experimental results with the Sigmajig test. Microstructure and hardness in the fusion zone of Sigmajig samples were measured. Based on the results, the following conclusions are drawn:

■ The CSI model predicted that the nominal and HiSi twitch would have the lowest susceptibility to solidification cracking. In contrast, the FRI model predicted that 5356 would have the greatest resistance, followed by the twitch alloys.
■ Results from the Sigmajig test showed that 5356 was the least susceptible to solidification cracking, followed by 4043, HiSi twitch, Nominal twitch, and finally 6061. The twitch alloys were found to be more susceptible to solidification cracking than predicted by the CSI and FRI models.
■ The fusion zone of the twitch materials showed large areas of oxide, which rose to the surfaces of welds and contributed to crack initiation and propagation.
■ The greater oxidation observed in the twitch alloys is likely from impurities in the powder core tubular wire used to make the samples, whereas all the other fillers were made from solid wire and did not show any oxides in the fusion zone. Powder core tubular wire is not ideal for aluminum alloys due to the propensity for oxide formation.
■ The hardness in the fusion zone of the two twitch alloys was substantially higher than that of 4043, 5356, and 6061.
■ It is expected that the susceptibility to solidification cracking of the twitch alloys will be significantly reduced with the use of solid wire, indicating that Al filler materials derived from the twitch scrap stream have the potential for desirable combinations of high hardness and good weldability.

Acknowledgements

The authors acknowledge support from the Center for Advanced Non-Ferrous Structural Alloys (CANFSA), a National Science Foundation Industry University Cooperative Research Center (IUCRC). The authors acknowledge Valimet for providing Al-Si and 2024 alloyed powders for this project.

Funding

Jamie Hamilton was supported by the U.S. Department of Education under a Graduate Assistance in Areas of National Need (GAANN) Fellowship (Grant #P200A210134). This material is based upon work supported by the National Science Foundation under Grant Number (2137243). Data analysis was supported by instrumentation acquired with support from the National Science Foundation (DMR-1828454).

References

1. Raabe, D., Ponge, D., Uggowitzer, P., Roscher, M., Paolantonio, M., Liu, C., Antrekowitsch, H., Kozeschnik, E., Seidmann, D., Gault, B. 2022. Making sustainable aluminum by recycling scrap: The science of "dirty" alloys. *Progress in Materials Science* 128. DOI: 10.1016/j.pmatsci.2022.100947.

2. Allwood, J. M., Cullen, J. M., Milford, R.L., 2010. "Options for Achieving a 50% Cut in Industrial Carbon Emissions by 2050. Environmental Science & Technology 44 (6): 1888-1894. DOI: 10.1021/es902909k.

3. Gutowski, T., Sahni, S., Allwood, J. M., Ashby, M. F., Worrell, E., 2013. The energy required to produce materials: constraints on energy-intensity improvements, parameters of demand. *Philosophical Transactions of the Royal Society A: Mathematical, Physical and Engineering Sciences* 371 (1986). DOI: 10.1098/rsta.2012.0003.

4. Ritchie, H., Rosado, P., 2023. CO_2 and Greenhouse Gas Emissions. *Our World in Data*.

5. Gautam, M., Pandey, B., Agrawal, M., 2018. Carbon Footprint of Aluminum Production: Emissions and Mitigation. *Environmental Carbon Footprints*, 197-228. Butterworth-Heinemann. DOI: 10.1016/B978-0-12-812849-7.00008-8.

6. International Aluminum Institute. 2024. Primary Aluminum Production.

7. Shankar, S., Gois, N., Molstad, E., Söderhjelm, C., Apelian, D., 2024. Upcycling of Low Quality Aluminum Automotive Scrap: The DNA of Twitch. *International Journal of Metalcasting*. DOI: 10.1007/s40962-024-01482-7.

8. Williams, K. C., Mallaburn, M. J., Gagola, M., O'Toole, M. D., Jones, R., Peyton, A. J., 2023. Classification of Shredded Aluminum Scrap Metal Using Magnetic Induction Spectroscopy. *Sensors* (Basel) 23 (18). DOI: 10.3390/s23187837.

9. Hamilton, J., Carsley, J. E., Klemm-Toole, J. 2025. Evaluating Welding Wire Fillers Derived from Scrap Aluminum. *Welding Journal*.

10. Kou, S. 2015. A criterion for cracking during solidification. *Acta Materialia* 88: 366-374. DOI: 10.1016/j.actamat.2015.01.034.

11. Kou, S. 2020. Welding Metallurgy. Wiley.

12. DebRoy, T., Wei, H. L., Zuback, J. S., Mukherjee, T., Elmer, J. W., Milewski, J. O., Beese, A. M., Wilson-Heid, A., De, A., Zhang, W., 2018. Additive manufacturing of metallic components - Process, structure and properties. *Progress in Materials Science* 92: 112-224. DOI: 10.1016/j.pmatsci.2017.10.001.

13. Soysal, T. 2025. Solidification crack susceptibility of 5xxx aluminum alloys. *Welding in the World*. DOI: 10.1007/s40194-025-01949-z.

14. Mossman, M. M., Lippold, J. C., 2002. Weldability Testing of Dissimilar Combinations of 5000- and 6000-Series Aluminum Alloys. *Welding Journal* 81 (9): 188-194.

15. Soysal, T., Kou, S., 2020. Role of liquid backfilling in reducing solidification cracking in aluminum welds. *Science and Technology of Welding and Joining* 25 (5): 415-421. DOI: 10.1080/13621718.2020.1732054.

16. Coniglio, N., Cross, C. E., 2009. Mechanisms for Solidification Crack Initiation and Growth in Aluminum Welding. *Metallurgical and Materials Transactions A* 40 (11): 2718-2728. DOI: 10.1007/s11661-009-9964-4.

17. Liu, J. and Kou, S. 2017. Susceptibility of ternary aluminum alloys to cracking during solidification. *Acta Materialia* 125: 513-523. DOI: 10.1016/j.actamat.2016.12.028.

18. Liu, J., Hu, P., Kou, S. 2023. A CFD Study on Intergranular Liquid Feeding and Cracking During Solidification in Welding. *Metallurgical and Materials Transactions A* 54 (11): 4342-4355. DOI: 10.1007/s11661-023-07169-8.

19. Matsuda, F., Nakata, K., Tsukamoto, K., Johgan, S., 1983. Effect of Additional Element on Weld Solidification Crack Susceptibility of Al-Zn-Mg Alloy (Report I): Results of Ring Casting Cracking Test. *Welding Research Institute of Osaka University*. DOI: 10.18910/9991.

20. Nagata, Y., Nakagawa, R., Kumaki, T., Matsushita, A., Yaguchi, K., Sakamoto, T., Orio, K., Okimura, Y., Okane, T., Muhammad, K.F., Yoshida, M., 2024. Novel Control Factor for Tensile Strength and Solidification Cracking in Partially Solidified Al-Mn-Cu Alloy Based on Campbell's Model with Fe-Rich Intermetallic Compounds. *Metallurgical and Materials Transactions A* 55 (11): 4462-4472. DOI: 10.1007/s11661-024-07564-9.

21. Coniglio, N., Cross, C. E., 2013. Initiation and growth mechanisms for weld solidification cracking. *International Materials Reviews* 58 (7): 375-397. DOI: 10.1179/1743280413Y.0000000020.

22. Kleindienst, J., Bagshaw, N., Iten, J., Klemm-Toole, J., 2025. Modeling Solidification Microstructure in an Inoculated Aluminum 6061 Alloy Processed with Gas Metal Arc Directed Energy Deposition. *JOM* 77 (3): 1423-1437. DOI: 10.1007/s11837-024-07066-4.

23. Yolcu, C. and Kahraman, F. 2023. How to avoid solidification cracking in arc welding of aluminum alloys: a review on weld metal grain refinement approaches. *Materials Research Express* 10 (12). DOI: 10.1088/2053-1591/ad16ab.

24. Kimura, R., Hatayama, H., Shinozaki, K., Murashima, I., Asada, J., Yoshida, M., 2009. Effect of grain refiner and grain size on the susceptibility of Al-Mg die casting alloy to cracking during solidification. *Journal of Materials Processing Technology* 209 (1): 210-219 DOI: 10.1007/s11837-003-0137-4.

25. Kou, S. 2003. Solidification and liquation cracking issues in welding. *JOM* 55 (6): 37-42. DOI: 10.1007/s11837-003-0137-4.

26. Giorjao, R., Sutton, B., Ramirez, A., 2021. New Composition Based Technique for Solidification Cracking Resistance Evaluation. *Metallurgical and Materials Transactions A* 52 (6): 2512-2521. DOI: 10.1007/s11661-021-06244-2.

27. Riffel, K., Marques, I. J., Leon-Henao, H., Ramirez, A. J., McCracken, S., Tatman, J., 2024. Computational Approach to Predict Solidification Cracking Susceptibility in Welding Filler Metals. *Advances in Materials, Manufacturing, and Repair for Power Plants*. DOI: 10.31399/asm.cp.epri2024p0924.

28. ASTM Standard B308M-20. 2021. Standard Specification for Aluminum-Alloy 6061-T6 Standard Structural Profiles. West Conshohocken, PA: ASTM International.

29. SAE International Material Specification. 2021. Aluminum Alloy, Welding Wire 5.2Si (4043). SAE Standard AMS4190L. DOI: org.mines.idm.oclc.org/10.4271/AMS4190L.

30. The Harris Products Group. n.d. Technical Specification Sheet: 5356 Aluminum Weld Wire.

31. ASM Aerospace Specification Metals Inc. n.d. Aluminum 6061-T6; 6061-T651. *ASM Aerospace Specifications Metals Inc.*

32. Goodwin, G.M. 1987. Development of a New Hot-Cracking Test - The Sigmajig. *Welding Journal* 33-s–38-s.

33. The Aluminum Association. 2002. Welding Aluminum: Theory and Practice. Arlington, V.A.

34. Gadallah, E., Abd El Aal, M., Mohamed, A. Y., El-Fahhar, H. H., 2023. Effects of filler on the microstructure and corrosion of similar and dissimilar gas inert tungsten arc welding aluminum alloys joints. *Scientific Reports* 13.

35. Fouad, R., Habba, M. I. A., Elshaghoul, Y. G. Y., El-Sayed Seleman, M. M., Hafez, K. M., Hamid, F. S., Barakat, W. S., 2024. The influence of various welding wires on microstructure, and mechanical characteristics of AA7075 Al-alloy welded by TIG process. *Scientific Reports* 14.

36. Liu, Y. 2017. Oxidation mechanism of micron-sized aluminum particles in Al-CO2 gradually heating system. ICSMME. DOI: 10.1088/1757-899X/248/1/012002.

37. Ali, R., Ali, F., Zahoor, A., Nawaz Shahid, R., Haq Tariq, N. U., Ali, G., Ullah, S., Shah, A., Bin. 2022. Preparatipn and oxidation of aluminum powders with surface alumina replaced by iron coating. *Journal of Energetic Materials* 40 (3) 243-257.

38. Awais, H., 2022. Preparation and oxidation of aluminum powders with surface alumina replaced by iron coating. *Journal of Energetic Materials* 40 (3): 243-257. DOI: 10.1080/07370652.2020.1859647.

JAMIE HAMILTON and **JONAH KLEMM-TOOLE** (*jklemmto@mines.edu)* are with Colorado School of Mines, Golden, Colo. **JOHN E. CARSLEY** is with The Novelis Global Research and Technology Center, Kennesaw, Ga.